Agricultural and Forest Meteorology 220 (2016) 207–215

Contents lists available at ScienceDirect

Agricultural and Forest Meteorology

journal homepage: www.elsevier.com/locate/agrformet

Short communication

Using distributed temperature sensing to monitor field scale dynamics of ground surface temperature and related substrate heat flux

V.F. Bense [a,*], T. Read [b], A. Verhoef [c]

[a] Department of Environmental Sciences, Wageningen University, Wageningen, Netherlands
[b] School of Environmental Sciences, University of East Anglia, Norwich, UK
[c] Department of Geography and Environmental Science, The University of Reading, UK

ARTICLE INFO

Article history:
Received 13 April 2015
Received in revised form 8 September 2015
Accepted 20 January 2016

Keywords:
Fibre-optic distributed temperature sensing
Temperature
Wet meadows
Thermal patterns
Vegetation structure
Energy balance closure

ABSTRACT

We present one of the first studies of the use of distributed temperature sensing (DTS) along fibre-optic cables to purposely monitor spatial and temporal variations in ground surface temperature (GST) and soil temperature, and provide an estimate of the heat flux at the base of the canopy layer and in the soil. Our field site was at a groundwater-fed wet meadow in the Netherlands covered by a canopy layer (between 0 and 0.5 m thickness) consisting of grass and sedges. At this site, we ran a single cable across the surface in parallel 40 m sections spaced by 2 m, to create a 40 m × 40 m monitoring field for GST. We also buried a short length (≈10 m) of cable to depth of 0.1 ± 0.02 m to measure soil temperature. We monitored the temperature along the entire cable continuously over a two-day period and captured the diurnal course of GST, and how it was affected by rainfall and canopy structure. The diurnal GST range, as observed by the DTS system, varied between 20.94 and 35.08 °C; precipitation events acted to suppress the range of GST. The spatial distribution of GST correlated with canopy vegetation height during both day and night. Using estimates of thermal inertia, combined with a harmonic analysis of GST and soil temperature, substrate- and soil-heat fluxes were determined. Our observations demonstrate how the use of DTS shows great promise in better characterizing area-average substrate/soil heat flux, their spatiotemporal variability, and how this variability is affected by canopy structure. The DTS system is able to provide a much richer data set than could be obtained from point temperature sensors. Furthermore, substrate heat fluxes derived from GST measurements may be able to provide improved closure of the land surface energy balance in micrometeorological field studies. This will enhance our understanding of how hydrometeorological processes interact with near-surface heat fluxes.

1. Introduction

1.1. Importance of the land surface thermal regime

The thermal regime at the land surface is the result of the interactions between vegetation, soil and atmosphere (e.g. transpiration, evaporation, soil water- and heat transfer). These processes are affected by micro-topography, local hydraulic and thermal properties, and radiative and structure parameters, such as canopy height and leaf area index (e.g. Moene and van Dam, 2014; Rodriguez-Iturbe et al., 1999). These complex interactions can be formalized via the energy balance, which is closely related to the water balance via the evapotranspiration term. The energy balance describes how the net radiation received at the land surface, R_n, is distributed between evapotranspiration (latent heat flux, LE), sensible heat flux, H, and substrate heat flux, G_{sub}. The latter flux concerns heat that gets stored in (during the day) or released from (night-time) a substrate layer, consisting of topsoil and leaf-litter.

However, some researchers consider a skin layer heat flux (e.g. Holtslag and de Bruin, 1988; Steeneveld et al., 2006), where the skin layer consists of vegetation, within-canopy air space, leaf litter and top soil, with related effective temperature: the skin temperature. Following a Fourier-type heat transfer law, the skin layer heat flux depends on 'skin conductivity' and the topsoil-skin temperature gradient. Skin conductivity is a complex parameter, that is affected by soil/vegetation thermal properties, within-canopy temperature profiles (affecting canopy heat storage) as well as by within-canopy aerodynamic transfer.

The substrate heat flux, G_{sub}, more generally referred to as surface soil heat flux, as both litter layer and canopy layer are often ignored (in particular for short canopies), is a particularly

* Corresponding author.
E-mail address: victor.bense@wur.nl (V.F. Bense).

http://dx.doi.org/10.1016/j.agrformet.2016.01.138
0168-1923/

important component of the land-surface energy balance under sparse or heterogeneous canopies. Whereas area-average estimates of the atmospheric fluxes (sensible and latent heat fluxes) can be reliably obtained from eddy covariance measurements, G_{sub} is commonly derived from a small number of point estimates, generally by using soil heat flux plates buried beneath the soil, combined with an estimate of heat storage above the plate, to yield an estimate of heat flux at the soil/substrate surface. Alternatively, G_{sub} can be determined from temperature measurements at or below the soil surface (e.g. Verhoef, 2004; Verhoef et al., 2012; van der Tol, 2012), as long as estimates of near-surface soil thermal properties are available. These temperatures are generally obtained using in-situ temperature probes installed (just) below the surface (e.g. Mayocchi and Bristow, 1995; Sauer and Horton, 2005). If leaf area index (LAI) varies considerably spatially, surface soil heat (substrate) flux estimates obtained at one or a few locations only may lead to poor energy balance closure ($R_n - G_{sub} \neq H + LE$), which is a widely observed phenomenon (Foken, 2008) that is not only caused by non-representative G_{sub} estimates, but can also be the result of atmospheric phenomena (e.g. advection).

The skin-, or land surface temperature (LST), plays a key role in all four energy balance fluxes. It is generally assumed to be a skin temperature to which the soil/litter layer (i.e. via the ground surface temperature, GST) and all canopy elements contribute, although with most of the signal coming from the top canopy layer. Quantifying the magnitude and spatial distribution of LST is important in micrometeorological and remote sensing studies, with the aim to further our understanding of the intricate functioning of natural or managed ecosystems. For example, through complex feedbacks the land surface thermal regime affects the spatial distribution of fauna and flora, and is a factor in controlling rates of primary production and biogeochemical processes. The spatial patterning of LST within a given habitat may provide thermal refugia for temperature sensitive species, enhancing the resilience of the ecosystem to short-term temperature maxima or minima (e.g. Ashcroft and Gollan, 2013).

LST can be monitored at the large scale using airborne thermal infrared techniques (e.g. Schmugge et al., 2002; Bertoldi et al., 2010). At an intermediate scale, ground based thermal infrared (IR) thermometers and cameras can be set up to monitor temperature variability over a scale of a few metres (Verhoef, 2004; Pfister et al., 2010), to hundreds of metres (Heinl et al., 2012). However, in the presence of a canopy layer, thermal IR imaging will only provide an effective skin temperature, with the uppermost canopy elements (e.g. sunlit top leaves) contributing most, so no explicit information on GST (i.e. at the base of the vegetation layer) will be available. Furthermore, LST, as well as GST, will be highly variable, in space as well as in time. To address this issue we need sensors that can measure temperatures in a spatially distributed and temporally near-continuous fashion.

Distributed temperature sensing (DTS) along fibre-optic cables, installed on the substrate surface or within the soil, provide a convenient means to obtain information on (the variability of) substrate and soil temperatures, e.g. for the verification of (below- and above-ground) multi-component soil-vegetation-atmosphere-transfer (SVAT) model outputs (e.g. Verhoef and Allen, 2000) for which separate measurements of vegetation and soil surface/substrate temperatures are required. Furthermore, line-averaged G_{sub} estimates, if the DTS temperature measurements are combined with measurements or estimates of thermal properties as mentioned above, would allow improved calculations of flux-partitioning when sensible heat flux is derived from scintillometry (Evans et al., 2012), whereas area-averaged estimates of G_{sub} (by using a horizontal multi-loop configuration) are more representative of flux tower footprint areas, and hence these are expected to lead to better energy balance closure than point-scale measurements with standard soil heat flux equipment. Hence, this paper aims to demonstrate the use of DTS technology in the determination of the spatio-temporal dynamics of soil- and near surface heat fluxes, and our purpose is not to advance the technology of DTS itself. As far as we are aware DTS has not been used for calculations of soil heat flux nor used to illustrate the implications of using a single measurement point as is practised widely in energy balance studies using a single heat flux plate (e.g. Wilson et al., 2002), to obtain soil heat flux for the determination of energy balance closure in heterogeneous canopies.

1.2. Distributed temperature sensing for monitoring ecosystem temperatures

Distributed temperature sensing (DTS) is being increasingly used for environmental temperature monitoring between the point and regional scale (e.g. Selker et al., 2006). DTS provides temperature measurements along an optical fibre at spatial intervals typically of around 1 m or less and temporal intervals of less than 1 min. The optical fibre can be configured into almost any spatial pattern such that a two- or three-dimensional space can be monitored for temperature from a single device. This approach, therefore has the potential to bridge the gap between point measurements which provide good temporal but poor spatial information, and remotely captured data which provide detailed spatial measurements but often poor temporal information. Furthermore, one continuous length of DTS cable can be partly placed on the soil and in the substrate, and within the canopy (at different heights, including near the canopy top to emulate IR-derived surface temperatures), thereby providing detailed information on GST and within-canopy temperature profiles, respectively.

The principle behind DTS is that a laser pulse is directed into a fibre optic cable and the intensity of backscattered photons arising from temperature dependent Raman scattering detected subsequently. Some photons return at higher frequencies, while others return at a lower frequencies. These are known as the anti-Stokes and Stokes intensities, respectively. The temperature, which more strongly affects the anti-Stokes signal, is computed from the ratio of these two intensities. For a more detailed explanation of the fundamental physical principles of the DTS method the reader is referred to Tyler et al. (2009).

A few examples exist of studies deploying DTS for monitoring temperature in natural or managed ecosystem applications. Krause et al. (2012) deployed DTS to investigate the extent to which invasive Rhododendron in a UK woodland modifies canopy temperatures. Similarly, Lutz et al. (2012) measured ground surface temperatures using DTS in both thinned and unthinned forests. In both cases the presence of a canopy was found to significantly moderate the ground surface temperature. These studies look at temperature along transects of cables; however, a two-dimensional configuration in the vertical was utilized by Thomas et al. (2011) to monitor atmospheric-surface layer flows by attaching the optical cable to a frame and system of pulleys. This type of approach (in the horizontal) is to our knowledge yet to be attempted for the monitoring of GST and the derivation of heat fluxes. To demonstrate how DTS can be used to map GST in relatively low canopies, how these temperatures are affected by canopy structure, and how such data can be used to obtain estimates of the spatiotemporal variation of substrate- and soil heat fluxes, we deployed a DTS system in a groundwater-fed meadow in the Netherlands.

2. Materials and methods

2.1. Field site and measurements of ground surface temperatures with DTS

The field site of De Maashorst Nature Reserve is located approximately 2 km southwest of the town of Uden in the southeast of the Netherlands (Fig. 1a). The site has a high ecological value and is an example of a groundwater-fed wet meadow. A shallow (<1 m) water table is maintained by the Peel Boundary Fault to the southwest of the site (Fig. 1b), which acts as a barrier to lateral groundwater flow (in this case, from northeast to southwest). The resultant strong vertical hydraulic gradient, and highly heterogeneous Quaternary cover sands, combine to give localized seepage, visible in aerial photographs of nearby cultivated fields and readily detectable in the agricultural drainage network of the area using temperature-based and hydrochemical methods (Bense and Kooi, 2004; Bonte et al., 2013).

At the study site, these localized seepage phenomena have resulted in a highly variable spatial distribution of plant species. Some regions are dominated by plants adapted for very moist conditions and are densely vegetated by for instance Reed Mannagrass (*Glyceria maxima*), Tufted Sedge (*Carex acuta*), Lesser Pond Sedge (*Carex acutiformis*), Marsh Horsetail (*Equisetum palustre*) and Marsh Marigold (*Caltha palustris*). Neighbouring areas can have much shorter and more sparse vegetation, including Churchyard Moss (*Rhytidiadelphus squarrosus*), Pointed Spear Moss (*Calliergonella cuspidate*), Calliergon Moss (*Calliergon cordifolium*), Thread Rush (*Juncus filiformis*), and Soft Rush (*Juncus effusus*), reflecting a greater depth to groundwater. In these systems the GST can be expected to be highly spatially organized, and be controlled by the structure (density, height and LAI) of the vegetation cover through variation in light extinction, as well as by its radiative, thermal and aerodynamic properties that affect the overall energy balance.

To measure the ground surface temperature, approximately 900 m length of steel armoured multimode fibre-optic cable (manufactured by Brugg Cables, http://www.bruggcables.com) was used. The fibre-optic cable we used had an outer blue polyamide jacket. This cable was laid out in a field directly adjacent to the Peel boundary fault zone (Fig. 1b). Here, fire-optic cable was installed in 21 parallel sections of 40 m length, with a 2 m spacing between each line. We refer to this area as the *monitoring field*. The cable was loosely secured to the ground, approximately every 2 m. This resulted in the cable sitting at slightly variable heights above the soil surface (Fig. 1c), estimated to be ranging between 0 and 10 cm. A ≈10 m long section (Fig. 1b; *buried cable section*) was buried to a depth of 10 ± 2 cm, and at the surface a parallel section of cable was installed of roughly equal length (Fig. 1d).

Temperature data were collected along the DTS cable continuously over a 48 h period (25-August and 26-August, 2009) using an Oryx DTS (Sensornet, Herts, UK), powered by a battery pack and charged by a solar panel. Data along the buried cable section were only collected on 26-August. Measurements were obtained over 1.01 m intervals along the cable with an integration time of 2.5 min, using a double-ended configuration (see van de Giesen et al. (2012) for a full explanation and description of the principle of double-ended DTS measurements). Using the double-ended DTS configuration a correction was made to the raw data for the differential attenuation of light along the fibre. To account for temperature offset and instrument drift, a 20 m section of coiled cable

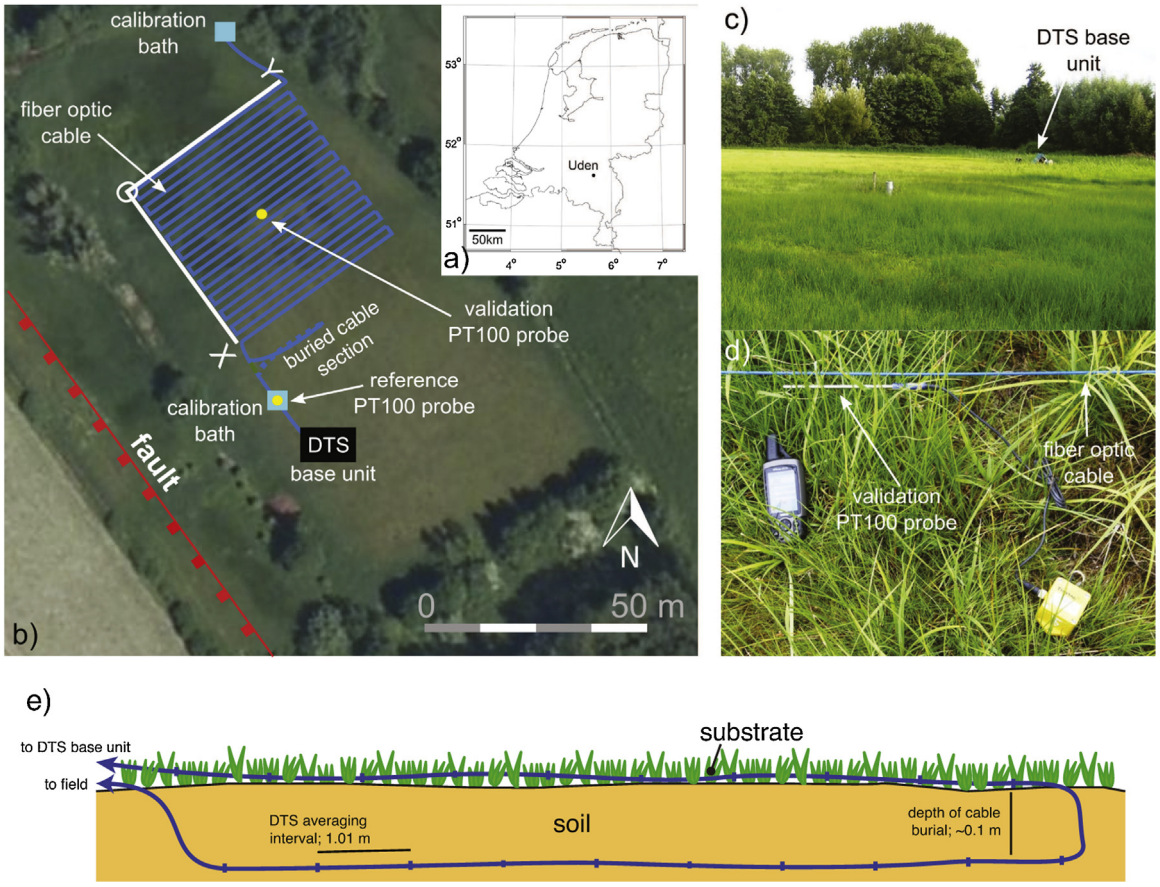

Fig. 1. (a) Location of the field site near the village of Uden, Netherlands, (b) the configuration of the DTS monitoring set-up, (c) wet meadow area where the fibre optic cable was deployed, and (d) validation PT100 probe adjacent to the fibre optic cable, (e) configuration of the buried cable section.

and a reference PT100 probe were placed in an insulating box filled with water. The DTS data were subsequently post-processed by comparing the average DTS coil temperature with the PT100 probe, and applying a time-varying offset. A second PT100 probe was placed in the centre of the field adjacent to the cable to validate the calibration procedure. Although the DTS derived temperatures were calibrated, following the procedure outlined above, it is likely that some discrepancies will still exist between ambient temperatures and those sensed along the fibres in the cable. This is due to heat absorption of the cable as a result of solar heating. Consequently, DTS temperatures can be higher than ambient during sunny periods of the day, whilst the magnitude of this effect is dependent on cable colour and thickness (de Jong et al., 2015). For the blue cable (diameter: 4 mm) we use in this study this bias might amount to up to 1–2 °C.

The variation in vegetation height was measured manually using a yardstick, to the nearest 5 cm, at 2 m intervals within the monitoring field. We consider that the vegetation height, albeit being a simple variable, should reflect well the LAI.

Meteorological data including air temperature and precipitation were obtained at hourly intervals from a weather station at Volkel, located at a distance of 6 km from the field site. At the field site, no meteorological data were collected.

2.2. Calculation of substrate- and soil heat flux from DTS measurements

We consider the *substrate* as that zone directly surrounding the above-ground DTS cable in the monitoring field where heat is stored in/released from and transferred to/from a substrate consisting of soil, above ground litter and fresh leaf matter and air (Fig. 1e). We employ the term *soil* in the conventional way and used the soil temperatures as measured in the buried cable section to calculate a soil heat flux at the depth of cable burial and the GST measurements to derive substrate heat flux.

The original 2.5 min averaged DTS temperature were averaged to give 30-minute average temperature values for each 1.01 m along the DTS cable. The temperature measurements were subjected to a harmonic analysis, which allowed calculation of substrate- and soil heat flux (G_{sub} and G_{soil}), using one estimate of average substrate thermal properties across the entire monitoring field, and that of the soil along the length of buried cable, respectively. We recognize that the thermal properties of the substrate and soil will be spatially variable, but we did not quantify this variability at our field site. For the soil, the texture and moisture content over a site will vary to a certain degree but at soil moisture contents above 50% of saturation (see Murray and Verhoef, 2007) this sensitivity is very strongly reduced. At our site with very shallow groundwater tables it is likely that soils are near saturation. Nevertheless, soil thermal properties could have been determined by using a heat-pulse needle probe, but substrate properties would have been impossible to obtain in this way due to lack of contact between probe and the bulk of the substrate, and there is currently no way of routinely obtaining such data in the field. We accept that for some locations we will overestimate or underestimate soil/substrate heat fluxes by assuming spatially constant thermal properties. However, we expect that the overall variability in heat fluxes would not change significantly if the detailed variability in thermal properties would have been known. This is because the biggest determinant of variability in diurnal peak value in heat fluxes is the amplitude of temperature which will be most strongly influenced by parameters like canopy properties, such as height and density, causing variations in shading, and within-canopy and near soil-surface aerodynamic resistances. Finally, high moisture contents in the capillary fringe and moisture fluxes due to root water uptake may affect the ground surface temperatures, but these effects are implicit in the temperature fluctuations and spatial distributions of temperature, hence they are already implicitly included in the soil heat flux as it is calculated following the methodology outlined below.

Substrate- and soil heat fluxes were calculated using the method described in Verhoef (2004) and Murray and Verhoef (2007). This involved a harmonic analysis of DTS temperatures, which was followed by calculation of the heat flux G [W m^{-2}] using an analytical method. This approach requires the estimation of thermal inertia (Γ [J m^{-2} K^{-1} s$^{-0.5}$]) for both the soil and the substrate. Γ is defined as $\sqrt{\lambda C_h}$ where λ [W m^{-1} K^{-1}] is thermal conductivity, and C_h [J m^{-3} K^{-1}] is volumetric heat capacity.

The soil type at the field site was peat and typical values of peat thermal properties were selected from the literature. For C_h, a value of 3×10^6 J m^{-3} K^{-1} was selected and thermal diffusivity, D_h, equalled 1.1×10^{-7} m^2 s^{-1} (near-saturation values derived from Table 1.2.4 in Grossnickle (2000)) which led to a thermal conductivity ($\lambda = D_h C_h$) of 0.33 W m^{-1} K^{-1}. In turn, this resulted in an estimate for soil thermal inertia, Γ_{soil}, of 995 J m^{-2} K^{-1} s$^{-0.5}$, which was used for the calculation of soil heat flux (G_{soil}), based on below ground DTS measurements.

However, the substrate also consisted of grass and air as it was impossible at the field site to have the fibre-optic cable touching the ground or leaf/litter surfaces throughout the entirety of its length. Nevertheless, this set-up provides a good approximation of the skin layer heat flux, as introduced in Section 1.1. With C_h for grass equal to 2.8×10^6 J m^{-3} K^{-1} (which is similar to peat) and $\lambda = 1.1$ W m^{-1} K^{-1} (Yaghoobian et al., 2010), we found $\Gamma = 1755$ J m^{-2} K^{-1} s$^{-0.5}$, whereas thermal inertia for air is 5.5 J m^{-2} K^{-1} s$^{-0.5}$. From visual estimates in the field we assume a substrate composition of about 35% air, 40% grass and 25% soil over each metre length of cable, hence $\Gamma_{substrate} = 955$ J m^{-2} K^{-1} s$^{-0.5}$.

With an estimate of thermal inertia we obtain a value for G using:

$$G = \Gamma \sum_{n=1}^{M} A_n \sqrt{n\omega} \left[\sin \left[n\omega t + \phi_n + \frac{\pi}{4} \right] \right] \quad (1)$$

where M is the total number of harmonics (n) used (20), A_n [°C] the amplitude of the nth harmonic, ϕ_n the phase shift of the nth harmonic, t [s] the time and ω is the angular frequency ($24 \times 60 \times 60$s). A_n and ϕ_n are derived from the harmonic analysis of DTS temperatures.

3. Results

3.1. Temporal ground surface temperature dynamics

The two full days (25-August and 26-August) covered by DTS measurements had contrasting meteorological conditions. On 25-August, rainfall overnight was followed by further rainfall approximately between 10:00 and 12:00 h (Fig. 2a). This totalled only 0.2 mm at the Volkel meteorological station. From 12:00 h, there was no further precipitation recorded at Volkel. The following day (26-August) was relatively warm and had been preceded by a cold night.

Fig. 2b plots the mean and range in GST across the monitoring field, as observed by DTS. Comparing these time series to those of air–temperature (Fig. 2a) shows that GST varies in a way similar to air temperature. Note that prior to the rainfall event on the 25-August, the GST is consistently below the air temperature at Volkel, and has a relatively small range (Fig. 2b). From approximately 20:00 on 25-August, the range in GST is in general much larger, except around 08:00 and 20:00 h when it reaches a minimum. Furthermore, the absolute value of GST is almost always higher than the air temperature during the day and lower at night.

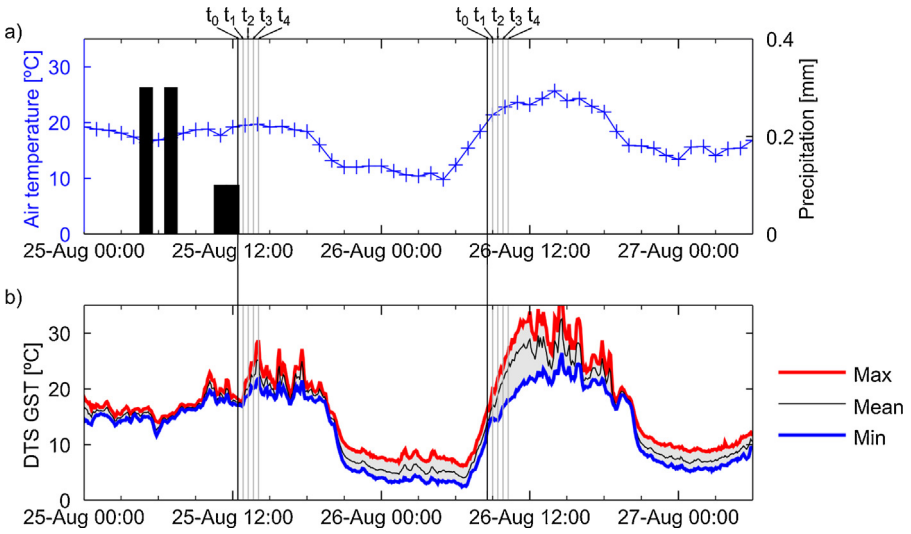

Fig. 2. (a) Air temperature and precipitation measured at Volkel and (b) time series of maximum, mean, and minimum GST recorded with the DTS along the fibre optic cable.

3.2. Spatial and temporal dynamics during warming

In order to investigate the spatiotemporal dynamics of GST across the monitoring field we selected two sequences from the entire data set. We consider the daytime temperature dynamics following the rainfall event on 25-August (between 10:00 h and 12:00 h), and compare this with the warming recorded during the morning of the following day with antecedent dry conditions. For every location along the cable, the difference in temperature (ΔGST), was calculated relative to the spatially averaged GST at reference times (t_0; Fig. 2a) of 12:25 h and 08:35 h on the 25th and 26th August, respectively. Values of ΔGST were calculated at four times (t_{1-4} after t_0, separated by 25 min, on both days. The ΔGST values were then spatially mapped onto a grid with 2 m spacing in the O-X direction, and 1 m spacing in the O-Y direction to replicate the spatial sampling interval in the field.

Fig. 3 shows the spatially mapped ΔGST values at the four times after t_0 on 25-August (a–d), and 26-August (e–h). On 25-August, there is little change in GST after the first 25 min. After this, both the range and mean ΔGST have increased - a trend which continues until 14:05 h. By now there is a spatial organization to the ΔGST which correlates with the vegetation height; the vegetation height is shown on each plot using contour lines. This correlation is further illustrated in Fig. 4. Those areas with the shortest vegetation, and hence with the lowest LAI, experience the greatest warming. On 26-August the initial warming is more rapid, and by 10:15 h there exists a pattern of ΔGST similar to that in vegetation height.

3.3. Impact of vegetation on GST dynamics

To investigate the effect of variable vegetation cover on the temperature dynamics, each DTS temperature measurement location was assigned to one of six groups according to vegetation height at that point. The group ranges were chosen such that the number of samples (n) in each group was as equal as possible, whilst still maintaining a distinct group which had the tallest vegetation only. The time series of average GST for each group was calculated, and the mean field temperature then subtracted to give the difference from the mean GST for each group (Fig. 4).

A clear diurnal signal emerges; areas with the lowest canopy height (<5 cm) are colder at night and warmer during the day, than those areas with tall (50–90 cm) vegetation (Fig. 4a). A transition, where the total range of GST is low, and the tallest vegetation regions switch from being the coldest to being the warmest regions, occur at 20:00 h on both days. The reverse happens at around 08:00 h on 26-August and to a lesser extent at around the same time on the previous day. The magnitude of the daytime vegetation shading effect is much reduced on 25-August, due to increased cloud cover which means there is less direct radiation reaching the canopy. A prevalence of diffuse radiation will lead to much less pronounced differences in GSTs between low and high crop height/LAI areas. In contrast, on a sunny day there would be distinct sunlit and shaded areas, due to considerable differences in radiation extinction, which is highly affected by LAI.

The presence of taller plant species has a clear moderating effect on the variation in GSTs. During August 26, at any point in the monitoring field the maximum of the range of diurnal GST variations was 35.08 °C while the minimum was 20.94 °C (Fig. 4b). The temperature range visually strongly correlates with the vegetation height ($r^2 = 0.48$), and is greatest where there is little or no vegetation cover.

Fig. 5 shows the observed temperatures in the buried cable section for 26-August. The temperatures along the cable show clearly where the cable enters the soil (Fig. 5a) at which point a transition zone occurs in which the temperatures recorded are in between those recorded at the surface (substrate) and in the soil (soil) (Fig. 5b). The data show that the spatial variation of temperature within each section (substrate and soil) is fairly low and varies slightly over time.

3.4. Substrate- and soil heat flux dynamics

The calculated spatiotemporal trends in substrate- and soil heat flux (G_{sub} and G_{soil}, respectively) are discussed for 26-August only, a day with a more clearly defined diurnal temperature signal than 25-August. Moreover, data for the buried cable section are only available for 26-August.

Fig. 6 shows the evolution of the calculated G_{sub} for 26-August (a predominantly sunny day, but with broken cloud occurrences in the afternoon) spatially averaged across the monitoring field, together with the G_{soil} in the buried section. Following standard behaviour of substrate and soil heat fluxes G_{sub} and G_{soil} vary diurnally, with negative values during the night and positive values between sunrise and sunset. For G_{sub} this denotes ground surface heat loss to and heat gain from the in-canopy air space, respectively; for G_{soil} these negative and positive fluxes are representative of heat loss

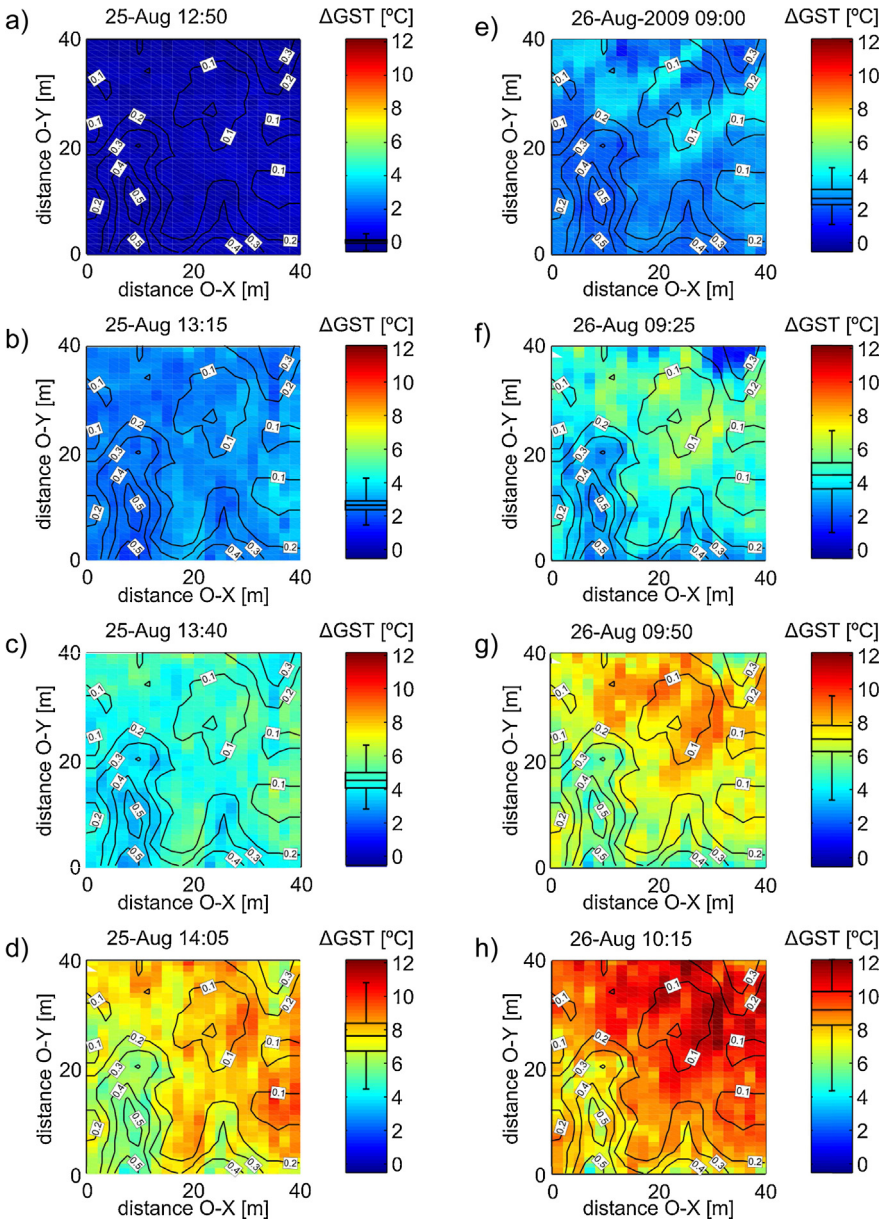

Fig. 3. (a–d) ΔGST distribution at 12:50 h (t_1; Fig. 2b), 13:15 h (t_2), 13:40 h (t_3), and 14:05 h (t_4) on 25-August, and (e–h) 09:00 h (t_1), 09:25 h, (t_2), 09:50 h (t_3), and 10:15 h (t_4) on 26-August. Each plot is overlaid with contour plots of the vegetation height [m]. The box plot in each colour bar gives the minimum, lower quartile, median, upper quartile, and maximum ΔGST.

to and heat gain from the soil layer above the below-ground DTS installation depth.

The magnitude of the substrate soil heat flux (peak value of around 190 W m^{-2}) fits with 26-August being a warm, predominantly sunny day and the substrate being relatively exposed (crop height <0.5 m and low LAI from visual inspection). Values of G_{sub} at their maximum (around 11:00 h) ranged between 76 W m^{-2} and 190 W m^{-2} with an average of 150 W m^{-2}, whereas for G_{soil} values between 17 and 36 W m^{-2} were found (average of 24 W m^{-2}). The soil heat flux values in the buried cable section peak around 12:00 h whilst the mean substrate heat fluxes across the field peaks earlier at 10:30–11:00 h. This reflects standard behaviour where the amplitude of diurnal variability is dampened in the soil, and a delay of peak values occurs.

Fig. 6b–d shows values of G_{sub} for 26-August, overlain by contours of vegetation height, to illustrate how G_{sub} varies considerably over the monitoring field over the duration of a day. Early in the day, at 05:00 h (Fig. 6b), all calculated G_{sub} values are negative indicating that the substrate is cooling. The more exposed areas are cooling more rapidly, indicated by a more negative G_{sub} in those parts of the field. At 11:00 h when values peak (Fig. 6c), the latter pattern is inverted to a degree where at this time of day the more exposed areas display the higher G_{sub} values. This is to be expected as the places where the canopy is sheltering the soil to a lesser degree, will have received more radiation and hence will exhibit larger substrate heat fluxes. Later in the day at 17:00 h (Fig. 6d) a similar pattern of G_{sub} arises as was present in the morning arises indicating that more exposed areas are cooling more rapidly than secluded areas. It is noticeable that in the afternoon of 26-August the mean and range in G_{sub} are strongly fluctuating at a time-scale of hours alternating between mean average and positive values. These cannot be directly attributed to fluctuations in air-temperature, which do not display such variability (Fig. 2), and most likely coincide with variations in incoming radiation.

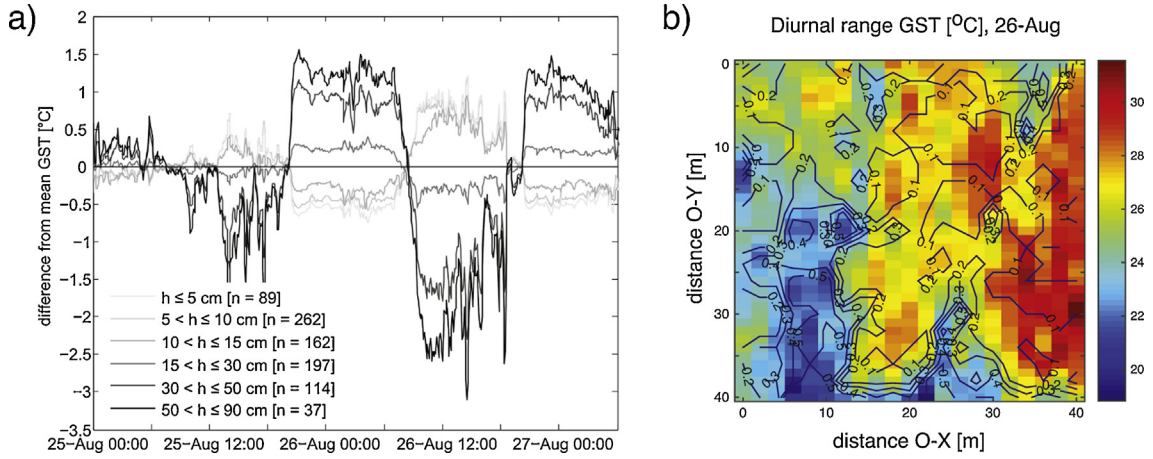

Fig. 4. (a) Difference between the mean GST relative to the temporal mean of the monitored area, for different vegetation height groupings. (b) The spatial variability of the diurnal range in GST on 26-August. The plot is overlaid with contours of the vegetation height [m].

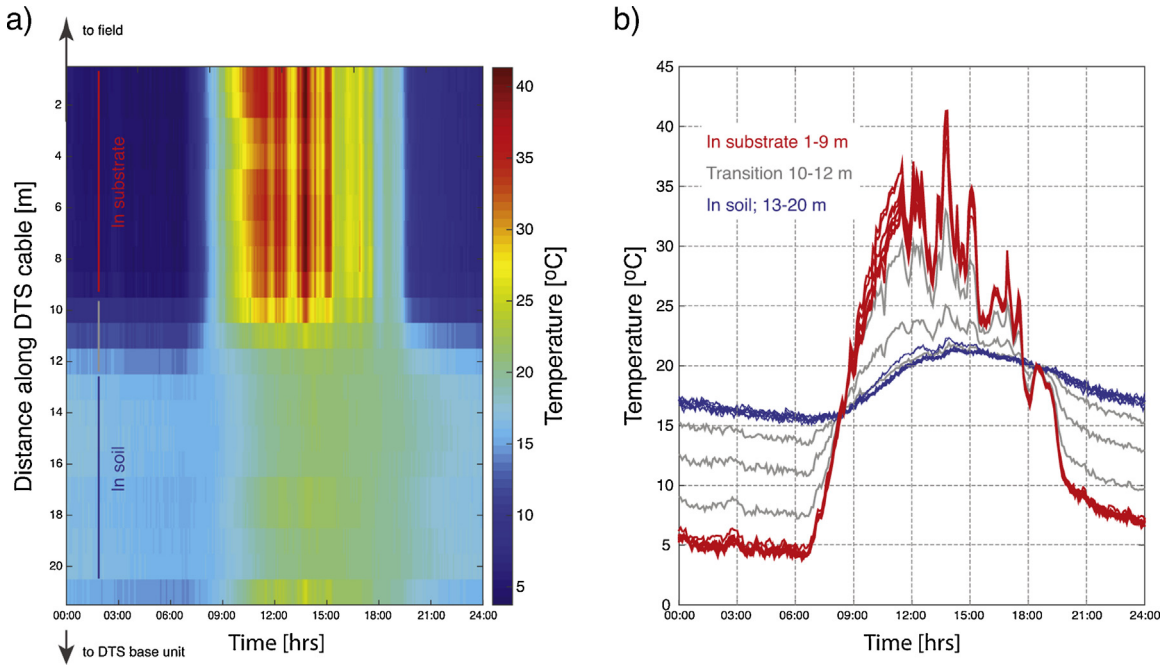

Fig. 5. (a) DTS temperature data for the buried cable section on 26-August. Location and set-up used to obtain these data are shown in Fig. 1a and d respectively. (b) DTS temperature in time for each part of the cable in the buried cable section. Data have a time resolution of 2.5 min.

4. Discussion and conclusions

We deployed distributed temperature sensing to monitor near surface temperatures in a wet meadow site in the Netherlands, in the late summer season. Using a relatively simple cable configuration, we were able to map considerable temperature patterns in great spatio-temporal detail. Temperature data like these, as we collected using DTS, would be practically impossible to collect with any other field methodology. In the discussion of our results we aim to separate spatial patterns and temporal dynamics present in our data.

The emerging spatial trends in the temperature data correlate with vegetation height, in particular, when the diurnal range of temperatures is considered (Fig. 4b), as well as for the calculated substrate heat fluxes (Fig. 6b–d). For taller vegetation, diurnal GST and G_{sub} variations are significantly smaller indicating that the thicker canopy more effectively dampens air temperature fluctuations. This results in temperatures that are higher underneath thicker vegetation during the night but relatively cool during daytime (Fig. 4a). These spatiotemporal differences in the diurnal range of GST and G_{sub} are a combination of radiative, aerodynamic and thermodynamic effects. Examples are a reduction in direct solar radiation (via canopy radiative extinction) received during the day and prevention of radiative cooling via long-wave outgoing radiation, and substrate heat loss driven by a temperature gradient between soil and substrate temperature, at night. When precipitation events occur these are observed to have an immediate temperature homogenizing effect which is largely independent of vegetation height (Figs. 2 and 3). This likely is the result of evaporation of intercepted water and the fact that radiation will be predominantly diffuse during and just after rainfall. Our data set allowed us to illustrate how the substrate surface temperature distribution evolves from such thermally homogeneous conditions which can either be caused by a rainfall event (Fig. 3a–d) or from the presence of dew in combination with the impact of diurnal incoming radiation temperature dynamics (Fig. 3e–h).

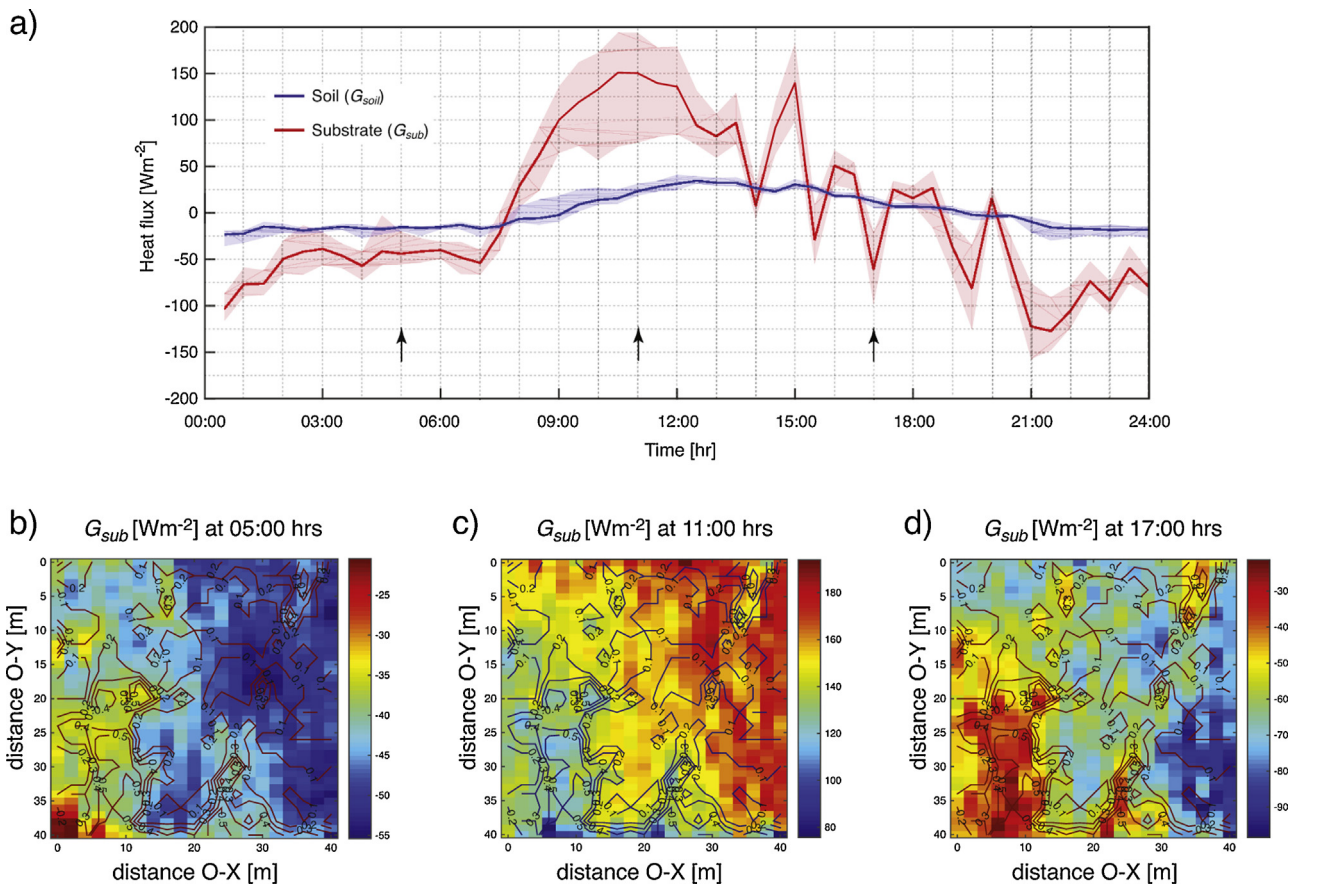

Fig. 6. (a) Substrate- and soil heat flux calculated for the field, and the buried cable section respectively, on 26-August. The mean heat flux values are indicated by the solid lines, while the range of the observed values is indicated by the shaded area. A total of 860 DTS observations were used to calculate the substrate heat flux at each 30 min time step, whilst for the soil heat flux in the BG section only 8 DTS observations were available (see Fig. 5). The arrows indicate the time steps for which the spatial distribution of the substrate heat fluxes are shown in (b–d). The spatial variability of G_{sub} is shown for (b) 05:00 h, (c) 11:00 h, and (d) 17:00 h. Each plot is overlaid with contours of the vegetation height [m].

In future studies, the collection of on-site auxillary data such as meteorological and independent heat flux observations will aid to understand correlations between observed temperature distributions and meteorological and soil conditions. However, we emphasize that even if such measurements at selected locations are obtained their use would be hampered by a series of issues. Temperature measurements with thermocouples or IR thermometers have their own particular problems such as radiation effects/contact issues with thermocouples, or lack of surface emissivity data for IR measurements. Furthermore, independent measurements of soil heat flux using soil heat flux plates should not be viewed as a 'standard' or reference method. They suffer as well from a range of shortcomings, such as interference with soil moisture flow, contact problems, and inaccuracies in the calculation of above-plate heat storage. These limitations reduce the usability of such data for the interpretation, or validation, of DTS derived temperatures and associated heat fluxes.

The DTS technique illustrated here also shows great promise in getting a better handle on area-average substrate and below-ground soil heat flux estimates, and their spatio-temporal variability, when the temperature measurements are combined with a harmonic analysis and subsequent calculation of soil heat flux with an analytical method (Verhoef, 2004). It seems that the heat flux directly at or below the soil surface can be obtained from DTS cables placed at the soil surface or buried in the soil, but the installation needs to be conducted very carefully. That is, the cable is either secured right against the soil/litter layer surface or the below-ground installation depth is known with as high a precision as possible. Verhoef (2004) and van der Tol (2012) have shown that the *surface* soil heat flux derived from soil temperatures, which requires a more complex analytical equation than Eq. (1) (see Verhoef, 2004: Eq. (6) and Verhoef et al., 2012: Eq. (9)) that uses C_h and D_h explicitly (rather than the composite thermal property, Γ), as well as the distance between the measurement location and the soil surface, is very sensitive to errors in the assumed installation depth. Furthermore, it would be preferable to install further parts of the cable at different heights throughout the canopy so that estimates of canopy heat storage can be obtained in the context of skin layer conductivity/skin layer heat transfer (see Section 1.1). Knowledge of the heat exchanged with or stored within the canopy would lead to significantly reduced errors in energy balance closure (Moderow et al., 2009).

We conclude that our DTS measurements have captured the temperature dynamics resultant from soil–vegetation–atmosphere energy exchanges in great spatial and temporal detail. However, in the absence of further experimental data such as field-average net radiation and sensible and latent heat fluxes, or within-field variation in leaf temperatures, it is not possible to evaluate the relative importance of different heat fluxes in this ecosystem, and interpret the DTS data in more detail, for example using SVAT modelling. In addition to the monitoring of these variables and fluxes in future studies, the DTS component can be expanded to include sections where the cable is buried into the soil, in order to potentially capture soil moisture dynamics as pioneered by Steele-Dunne et al. (2010). Shading effects could be further evaluated by using white and black jacketed fibre-optic cables in a similar way as described

by Petrides et al. (2011) who studied shading over stream channels using DTS.

Also, in the present study, we only look at two-dimensional spatial variation in temperature. However, it is possible to configure the cable such that any geometry in space may be monitored. This could be made to include the soil, canopy, and above canopy at a number of different heights. It is also possible, by coilling the fibre optic cable around a vertical cylinder, for example, to increase the effective spatial resolution (e.g. Vogt et al. (2010) for a stream bed and van Emmerik et al. (2013) for a lake application). When considering the energy balance at the land surface, and in particular the role of within-canopy storage, several of these high resolution vertical profiles could be included, as part of the same fibre optic cable.

Moreover, ground based- (e.g. Cardenas et al., 2008; Pfister et al., 2010) or airborne thermal imaging (e.g. Richter et al., 2009), mostly capturing the temperature of surface elements at or near the top of the canopy, can be combined with DTS which in our set-up monitors temperatures inside the canopy. This may lead to more accurate estimates of sensible heat flux when this flux is determined from bulk transfer equations, that rely on a surface-air temperature gradient. Although our field campaign was limited to only a few days at the end of the summer season (late August); longer term monitoring would yield further information on the temperature effects of vegetation dynamics in terms of the energy balance, but also in the context of soil respiration, for example, as this is strongly affected by seasonal changes in soil temperature and presence of vegetation (vigorous root growth/respiration during summer, versus winter vegetation dormancy with microbial respiration only). All of these efforts would further our understanding of the interactions between near-surface heat flow dynamics and ecohydrological processes.

Acknowledgement

Nico Ettema of the Institute for Nature Education and Sustainability, Uden, Netherlands is thanked for valuable advice during field work. The research reported in this paper was supported by a Natural Environment Research Council (NERC) studentship (NE/J500069/1) to Tom Read. Data underlying this research can be provided upon request by contacting the corresponding author.

References

Ashcroft, M.B., Gollan, J.R., 2013. Moisture, thermal inertia, and the spatial distributions of near-surface soil and air temperatures: understanding factors that promote microrefugia. Agric. Forest Meteorol. 176, 77–89.
Bense, V.F., Kooi, H., 2004. Temporal and spatial variations of shallow subsurface temperature as a record of lateral variations in groundwater flow. J. Geophys. Res. B: Solid Earth 109 (4).
Bertoldi, G., Notarnicola, C., Leitinger, G., Endrizzi, S., Zebisch, M., Della Chiesa, S., Tappeiner, U., 2010. Topographical and ecohydrological controls on land surface temperature in an alpine catchment. Ecohydrology 3 (2), 189–204.
Bonte, M., Geris, J., Post, V., Bense, V., van Dijk, H., Kooi, H., 2013. Mapping surface water–groundwater interactions and associated geological faults using temperature profiling. In: Groundwater and Ecosystems of IAH Series on Hydrogeology, chapter 8, pp. 81–94.
Cardenas, B., Harvey, J., Packman, A., Scott, D., 2008. Ground-based thermography of fluvial systems at low and high discharge reveals potential complex thermal heterogeneity driven by flow variation and bioroughness. Hydrol. Process., 22.
de Jong, S.A.P., Slingerland, J.D., van de Giesen, N.C., 2015. Fiber optic distributed temperature sensing for the determination of air temperature. Atmos. Measur. Techn. 8, 335–339.
Evans, J.G., McNeil, D., Finch, J.W., Murray, T., Harding, R.J., Ward, H., Verhoef, A., 2012. Determination of turbulent heat fluxes using a large aperture scintillometer over undulating mixed agricultural terrain. Agric. Forest Meteorol. 166–167, 221–233.
Foken, T., 2008. The energy balance closure problem: an overview. Ecol. Appl. 18, 1351–1367.
Grossnickle, S., 2000. Ecophysiology of Northern Spruce Species: The Performance of Planted Seedlings. NRC Research Press.
Heinl, M., Leitinger, G., Tappeiner, U., 2012. Diurnal surface temperature regimes in mountain environments. Phys. Geogr. 33 (4), 344–359.
Holtslag, A.A.M., de Bruin, H., 1988. Applied modelling of the night-time surface energy balance over land. Boundary-Layer Meteorol. 27, 689–704.
Krause, S., Taylor, S.L., Weatherill, J., Haffenden, A., Levy, A., Cassidy, N.J., Thomas, P., 2012. Fibre-optic distributed temperature sensing for characterizing the impacts of vegetation coverage on thermal patterns in woodlands. Ecohydrology.
Lutz, J.A., Martin, K.A., Lundquist, J.D., 2012. Using fiber-optic distributed temperature sensing to measure ground surface temperature in thinned and unthinned forests. Northwest Sci. 86 (2), 108–121.
Mayocchi, C., Bristow, K., 1995. Soil surface heat flux: some general questions and comments on measurements. Agric. Forest Meteorol. 75, 43–50.
Moderow, U., Aubinet, M., Feigenwinter, C., Kolle, O., Lindroth, A., Molder, M., Montagnani, L., Rebmann, C., Bernhofer, C., 2009. Available energy and energy balance closure at four coniferous forest sites across Europe. Theor. Appl. Climatol. 98 (3-4), 397–412.
Moene, A., van Dam, J., 2014. Transport in the Atmosphere-Vegetation-Soil Continuum. Cambridge University Press.
Murray, T., Verhoef, A., 2007. Moving towards a more mechanistic approach in the determination of soil heat flux from remote measurements: i. A universal approach to calculate thermal inertia. Agric. Forest Meteorol. 147, 80–87.
Murray, T., Verhoef, A., 2007. Moving towards a more mechanistic approach in the determination of soil heat flux from remote measurements: ii. Diurnal shape of soil heat flux. Agric. Forest Meteorol. 147, 88–97.
Petrides, A., Huff, J., Arik, A., van de Giesen, N., Kennedy, A.M., Thomas, C.K., Selker, J.S., 2011. Shade estimation over streams using distributed temperature sensing. Water Resour. Res. 47, W07601.
Pfister, L., McDonnell, J.J., Hissler, C., Hoffmann, L., 2010. Ground-based thermal imagery as a simple, practical tool for mapping saturated area connectivity and dynamics. Hydrol. Pro 21, 3123–3132.
Richter, K., Palladino, M., Vuolo, F., Dini, L., D'Urso, G., 2009. Spatial distribution of soil water content from airborne thermal and optical remote sensing data. In: Proceedings of SPIE – The International Society for Optical Engineering, p. 7472.
Rodriguez-Iturbe, I., D'Odorico, P., Porporato, a., Ridolfi, L., 1999. On the spatial and temporal links between vegetation, climate, and soil moisture. Water Resour. Res. 35 (12), 3709.
Sauer, T.J., Horton, R., 2005. Soil heat flux. In: Micrometeorology in Agricultural Systems, vol. 47 of Agronomy Monograph, pp. 131–154, chapter 7.
Schmugge, T., Kustas, W., Ritchie, J., Jackson, T., Rango, A., 2002. Remote sensing in hydrology. Advances in Water Resources 25 (8–12), 1367–1385.
Selker, J., Thévenaz, L., Huwald, H., Mallet, A., Luxemburg, W., Van De Giesen, N., Stejskal, M., Zeman, J., Westhoff, M., Parlange, M., 2006. Distributed fiber-optic temperature sensing for hydrologic systems. Water Resour. Res. 42 (12).
Steele-Dunne, S., Rutten, M., Krzeminska, D., Hausner, M., Tyler, S., Selker, J., Bogaard, T., Van De Giesen, N., 2010. Feasibility of soil moisture estimation using passive distributed temperature sensing. Water Resour. Res. 46, W03534.
Steeneveld, G., van de Wiel, B., Holtslag, A., 2006. Modeling the evolution of the atmospheric boundary layer coupled to the land surface for three contrasting nights in cases-99. J. Atmos. Sci. 63, 920–935.
Thomas, C.K., Kennedy, A.M., Selker, J.S., Moretti, A., Schroth, M.H., Smoot, A.R., Tufillaro, N.B., Zeeman, M.J., 2011, November. High-resolution fibre-optic temperature sensing: a new tool to study the two-dimensional structure of atmospheric surface-layer flow. Boundary-Layer Meteorol., 177–192.
Tyler, S.W., Selker, J.S., Hausner, M.B., Hatch, C.E., Torgersen, T., Thodal, C.E., Schladow, S.G., 2009, January. Environmental temperature sensing using Raman spectra DTS fiber-optic methods. Water Resour. Res. 45, 1–11.
van de Giesen, N., Steele-Dunne, S.C., Jansen, J., Hoes, O., Hausner, M.B., Tyler, S., Selker, J., 2012. Double-ended calibration of fiber-optic Raman spectra distributed temperature sensing data. Sensors, 5471–5485.
van der Tol, C., 2012. Validation of remote sensing of bare soil ground heat flux. Remote Sens. Environ. 121, 275–286.
van Emmerik, T., Rimmer, a., Lechinsky, Y., Wenker, K., Nussboim, S., van de Giesen, N., 2013. Measuring heat balance residual at lake surface using distributed temperature sensing. Limnol. Oceanogr. Methods 11 (1991), 79–90.
Verhoef, A., 2004. Remote estimation of thermal inertia and soil heat flux for bare soil. Agric. Forest Meteorol. 123, 221–236.
Verhoef, A., Allen, S., 2000. A SVAT scheme describing energy and CO_2 fluxes for multi-component vegetation: calibration and test for a Sahelian Savannah. Ecol. Model. 127, 245–267.
Verhoef, A., Ottle, C., Cappelaere, B., Murray, T., Saux-Picart, S., Zribi, M., Maignan, F., Boulain, N., Demarty, J., Ramier, D., 2012. Spatio-temporal surface soil heat flux estimates from satellite data; results for the AMMA experiment at the Fakara (Niger) supersite. Agric. Forest Meteorol. 154–155, 55–66.
Vogt, T., Schneider, P., Hahn-Woernle, L., Cirpka, O.A., 2010. Estimation of seepage rates in a losing stream by means of fiber-optic high-resolution vertical temperature profiling. J. Hydrol. 380 (1–2), 154–164.
Wilson, K.B., Goldstein, A.H., Falge, E., Aubinet, M., Baldocchi, D., Berbigier, P., Bernhofer, C., Ceulemans, R., Dolman, H., Field, C., Grelle, A., Law, B., Meyers, T., Moncrieff, J., Mon-son, R., Oechel, W., Tenhunen, J., Valentini, R., Verma, S., 2002. Energy balance closure at FLUXNET sites. Agric. Forest Meteorol. 113, 223–243.
Yaghoobian, N., Kleissl, J., Krayenhoff, E., 2010. Modeling the thermal effects of artificial turf on the urban environment. J. Appl. Meteor. Climatol. 49, 332–345.